Accepted Manuscript

The sequence and kinetics of pre-precipitation in Mg-Nd alloys after HPT processing: A synchrotron and DSC study

Yousf Islem Bourezg, Hiba Azzeddine, Louis Hennet, Dominique Thiaudière, Yi Huang, Djamel Bradai, Terence G. Langdon

PII: S0925-8388(17)31760-7

DOI: 10.1016/j.jallcom.2017.05.166

Reference: JALCOM 41896

To appear in: *Journal of Alloys and Compounds*

Received Date: 11 January 2017

Revised Date: 4 April 2017

Accepted Date: 15 May 2017

Please cite this article as: Y.I. Bourezg, H. Azzeddine, L. Hennet, D. Thiaudière, Y. Huang, D. Bradai, T.G. Langdon, The sequence and kinetics of pre-precipitation in Mg-Nd alloys after HPT processing: A synchrotron and DSC study, *Journal of Alloys and Compounds* (2017), doi: 10.1016/j.jallcom.2017.05.166.

Revised to Journal of Alloys and Compounds (April 2017)

The sequence and kinetics of pre-precipitation in Mg-Nd alloys after HPT processing: A synchrotron and DSC study

Yousf Islem Bourezg[a], Hiba Azzeddine[a,b,*], Louis Hennet[c], Dominique Thiaudière[d], Yi Huang[e], Djamel Bradai[a], Terence G. Langdon[e]

[a] Faculty of Physics, USTHB, Algiers, Algeria.
[b] Department of Physics, University of M'sila, M'sila, Algeria.
[c] Conditions Extrêmes et Matériaux : Haute Température et Irradiation, CNRS-CEMHTI, 1D Ave de la Recherche Scientifique, 45071 Orléans Cedex 2, France
[d] Synchrotron SOLEIL, L'Orme des Merisiers, Saint-Aubin, 91192 Gif-sur-Yvette Cedex, France
[e] Materials Research Group, Faculty of Engineering and the Environment, University of Southampton, Southampton SO17 1BJ, UK

Abstract

The sequence and kinetics of pre-precipitation in an Mg-1.43Nd (wt.%) alloy was investigated after severe plastic deformation by high-pressure torsion (HPT) at room temperature using *in situ* synchrotron X-ray diffraction and differential scanning calorimetry (DSC). *In situ* aging at 250°C up to 5 h led to precipitation of the β_1-Mg_3Nd and β-$Mg_{12}Nd$ phases but without any evidence for the metastable β‴(undifferentiated β″-DO19 and β'-Mg_7Nd) or equilibrium β_e-$Mg_{41}Nd_5$ phases. The β_1-Mg_3Nd and β-$Mg_{12}Nd$ phases appeared rapidly after HPT processing and their amounts were relatively large compared to the non-deformed sample. The Avrami time exponent of the β-$Mg_{12}Nd$ phase had a value near unity indicating a mechanism of nucleation after saturation and growth of the particles in 2 dimensions. DSC analysis revealed all metastable phases as well as the equilibrium phase. The activation energies associated with the pre-precipitation phases ranged between ~126 and ~235 kJ mol^{-1}.

Keywords: differential scanning calorimetry; high-pressure torsion; Mg-Nd alloy; precipitation; synchrotron X-ray diffraction.

Corresponding author: Hiba Azzeddine, e-mail: azehibou@yahoo.fr

1. Introduction

Magnesium-rare earth (RE) alloys have received much attention recently in the automotive and aerospace industry due to their corrosion resistance, better room temperature formability and relative high strength [1–3]. Such strengthening was attributed to a distribution of plate-shaped or lath-rod-shaped precipitates of intermediate or equilibrium phases formed parallel or normal to the basal plane of the magnesium matrix phase [2]. It was shown that die-cast Mg-RE (RE = Nd, Ce, La) alloys exhibit high creep resistance (at 177 °C) with the Mg–Nd alloys being the most creep-resistant. This temperature is close to the mean operating temperatures (150–200 °C) for powertrain applications, namely, the transmission case and the engine block [4, 5]. Such creep resistance of die-cast Mg–RE alloys was associated with mechanism of strengthening of α-Mg matrix by solid solution and/or precipitation [4, 5]. Furthermore, the strength of Mg-Nd alloys may be enhanced through solid solution strengthening and subsequent thermo-mechanical treatments [6].

Severe plastic deformation (SPD) techniques, such as equal-channel angular pressing (ECAP) [7], accumulative roll bonding (ARB) [8] and high-pressure torsion (HPT) [9], have the potential not only to produce ultrafine-grained (UFG) microstructures [10–13] but also to significantly affect the size and distribution of precipitates within the matrix [14]. They have also a great influence on the sequence and kinetics of precipitation in alloys [15]. This is generally attributed to the extra dislocations introduced into the matrix by SPD which accordingly provides additional nucleation sites for precipitation.

The general precipitation sequence for binary Mg-Nd alloys was reported as follows: SSS → GP zones → β''-Mg_3Nd → β'-Mg_7Nd → β_1-Mg_3Nd → β-$Mg_{12}Nd$ → β_e-$Mg_{41}Nd_5$ [2, 16] but recently the following precipitation sequence was proposed: SSS → GP zones (N, V, hexagon) → β''' → β_1 (fcc, Mg_3Nd) → β (tetragonal, $Mg_{12}Nd$) → β_e (tetragonal, $Mg_{41}Nd_5$) [17]. It was considered that the β''' phase includes the β''-Mg_3Nd and β'-Mg_7Nd phases and

ranges in composition from $x_{Nd} = 0.125$ to $x_{Nd} \approx 0.166$. The orientation relationship between the β" (with an ordered DO19 structure) and α-Mg phase was such that $[0001]_{\beta"}$ //$[0001]_{\alpha}$ and $\{2\bar{1}\bar{1}0\}_{\beta"}$ //$\{2\bar{1}\bar{1}0\}_{\alpha}$. While that of the β'-$Mg_7Nd$ (with an orthorhombic structure) was $[100]_{\beta'}$ //$[1210]_{\alpha}$ and $\{001\}_{\beta'}$ //$\{0001\}_{\alpha}$. The β_1-Mg_3Nd phase has the crystallographic relationship $[001]_{\beta1}$ // $[11\bar{2}0]_{\alpha}$ and $\{110\}_{\beta1}$ //$\{1102\}_{\alpha}$. The orientation relationship between β-$Mg_{12}Nd$ and the matrix was reported to be the following: $[0002]_{\beta}$ //$[10\bar{1}0]_{\alpha}$ and $\{10\bar{1}0\}_{\beta}$ //$\{0001\}_{\alpha}$ and finally the β_e-$Mg_{41}Nd_5$ equilibrium phase is fully non-coherent with the matrix [18]. The morphologies and compositions of the metastable phases in the early stage of Mg-Nd alloy aging were the focus of some recent studies using high-angle annular dark field scanning transmission electron microscopy (HAADF-STEM) and/or atom probe tomography analysis [16, 17, 19, 20]. However, except only for a single pioneering investigation [6], there was very little attempt to quantify the pre-precipitation and precipitation kinetics in Mg-Nd alloys either after conventional deformation or after processing by SPD. Accordingly, the aim of this work was to investigate the decomposition kinetics of pre-precipitation in an Mg-1.43Nd (wt.%) alloy after SPD processing by HPT using *in situ* synchrotron X-ray diffraction and differential scanning calorimetry (DSC) analysis.

2. Experimental material and procedures

The Mg-1.43Nd (wt.%) alloy samples were provided in an as-cast state by colleagues from the Institut für Metallkunde und Metallphysik (IMM), Aachen, Germany. The as-cast alloy was subjected to a solution annealing at 535 °C for 6 h followed by quenching into water. Several cylindrical rods were machined from the initial blocks with diameters of 10 mm and lengths of 50 mm. For HPT processing, disks were sliced from the rods with thicknesses of ~0.9 mm and these disks were then inserted into an HPT facility. These disks

were processed at room temperature (RT) through totals of ½, 1, 5 and 10 turns using an imposed pressure of 6.0 GPa, a rotational speed of 1 rpm and quasi-constrained conditions where there is a small outflow of material around the periphery of the disk during the straining operation [21]. After processing, the disck were heated in an Anton-Paar furnace without any protective atmosphere at 250 °C for 5 h in order to clarify the precipitation sequence. These disks were subjected to X-ray diffraction on the DIFFABS beamline at the SOLEIL synchrotron (Gif-sur-Yvette, France) by illuminating with a monochromatic X-ray beam at an energy of 9 keV (0.1377 nm). A 2D X-ray hybrid pixel detector (XPAD-S140) was used in order to analyze the early stages of precipitation with the detector recording the patterns every 0.025 s. The recorded 2D spots were integrated into 1D diffractograms using in-house software at the DIFFABS beamline. In order to compare the precipitation behavior, some solution treated samples were aged at 250 °C for 5 h without HPT processing.

Differential scanning calorimetry (DSC) analysis of the Mg-1.43Nd (wt.%) alloy after solid solution and HPT processing was performed using a 2920 MDSC calorimeter under a nitrogen atmosphere with a pressure of 1 bar. Specimens of 18−20 mg were cut near the centers of the disks and placed in an aluminum crucible (6.5 mm inner diameter and 1 mm height) for introduction into the DSC furnace, while an empty Al crucible was used as a reference. Four heating rates (5, 10, 20 and 30 °C/min) were applied in the DSC experiments over a temperature range from 80 to 500 °C.

3. Experimental results

3.1. In situ synchrotron XRD

Figure 1 presents the X-ray diffraction patterns of the Mg-1.43Nd (wt.%) alloy after solution annealing at 535 °C for 6 h and *in situ* aging at 250 °C to 5 h. The first XRD pattern shows the presence of 3 peaks of the Mg matrix together with another peak which appears to

belong to the β-$Mg_{12}Nd$ phase. As the *in situ* ageing time increases, a new peak appears at 2θ = 21.45° indexed as the β_1-Mg_3Nd phase. It is clear that the amount of the β-$Mg_{12}Nd$ phase increases as new peaks develop near 2θ = 21.67° and 29.32°. The peak of the β_1-Mg_3Nd phase near 2θ = 21.45° was observed shortly after 6 min aging while much longer times of up to 160 min were required for appearance of the β-$Mg_{12}Nd$ peak.

Figures 2 and 3 show the X-ray diffraction patterns of the Mg-1.43Nd (wt.%) after HPT processing to 1 and 10 turns, respectively, obtained during *in situ* ageing at 250 °C to 5 h. The amount of the β_1-Mg_3Nd and β-$Mg_{12}Nd$ phases (which is directly proportional to the intensity) during the *in situ* aging is larger after HPT processing compared to the non-deformed state (Fig. 1) and it also increases with increasing strain. The peaks of the β_1-Mg_3Nd precipitate in the sample deformed after 1 HPT turn appear after 5 min annealing at 250 °C and their intensity increases until 98 min and then decreases up to 5 h. These peaks develop more rapidly (~3 min) for samples deformed after 10 HPT turns as shown in Fig. 3. Furthermore, their intensity decreases from 67 min and there is a full dissolution after 5 h of annealing at 250 °C. The relative error of the shortest apparition time of any precipitate was estimated as ~ 0.013 %. Therefore, such a low relative error does not alter considerably the kinetics. Concerning the β-$Mg_{12}Nd$ phase, Figs 2 and 3 show that its associated peaks appear after 56 and 50 min of annealing for samples deformed up to 1 and 10 HPT turns, respectively, and their intensities show a continuous increase with increasing ageing time.

3.2 DSC analysis

Figure 4 presents the DSC curves of Mg-1.43Nd (wt.%) after solid solution annealing and HPT processing to 1 and 10 turns obtained at a heating rate of 30 °C/min. A first exothermic peak is visible around 180 °C in the DSC curves of the 1 and 10 HPT samples and this corresponds to a recrystallization process. A second exothermic signal around 220 °C is assigned to the precipitation of the β’’’(undifferentiated β’’-DO19 and β-Mg_7Nd) phases.

Their subsequent dissolution is recognized by the endothermic peak D_1 around 250 °C as is evident in Fig. 4. The third exothermic peak corresponds to the precipitation of the β_1-Mg_3Nd phase, followed by precipitation of β-$Mg_{12}Nd$ as shown by the appearance of a fourth exothermic peak. The endothermic peak D_2 around 400 °C is the signature for the dissolution of the β_1-Mg_3Nd and β-$Mg_{12}Nd$ phases. The last exothermic peak is associated with the equilibrium precipitate phase β_e-$Mg_{41}Nd_5$. In general, these observations are in good agreement with the precipitation sequence reported earlier [17].

The activation energies associated with the precipitation of β’’’, β_1-Mg_3Nd and β-$Mg_{12}Nd$ phases were estimated from the DSC curves using the Boswell method [22]:

$$\ln \frac{V}{T_p} = C - \frac{E}{RT_p} \quad (1)$$

where V is the heating rate, E is the activation energy, T_p is the maximum temperature of the peak, R is the universal constant of gases and C is a constant. As is evident from Fig. 5, the Boswell plots for the β’’’phase, β_1-Mg_3Nd and β-$Mg_{12}Nd$ phases, respectively, yield straight lines and the activation energies are determined from the slopes of these plots. The values of activation energies for different precipitates phases are given in Table 1.

4. Discussion

4.1 Sequence of precipitation in the Mg-Nd alloy

The *in situ* synchrotron X-ray diffraction patterns of the non-deformed and deformed Mg-1.43 Nd (wt.%) alloy aged at 250 °C for 5 h (Figs 1–3) were not able to detect the peaks of the β”-Mg_3Nd or β’-Mg_7Nd phases during the early stage of annealing. Furthermore, the DSC analysis shown in Fig. 4 reveals a sequence of precipitation that is consistent with a recent proposal [17]. In the present investigation, the use of high energy X-ray analysis failed to detect these phases in the alloy. Usually, investigations of the precipitation evolution in the

early stages of annealing in Mg-Nd alloys may be undertaken in specimens isothermally annealed over the temperature range 170–190 °C [16, 17, 19]. In this range of annealing temperatures, the diffusivity of Nd in Mg is very low (~10^{-22} m^2/s at 177 °C) [19], thereby permitting a convenient tracking of precipitation during the very early stage of annealing. Indeed, it was reported that aging at temperature above 200 °C of Mg-2.35Nd (wt.%) alloy caused a rapid dissolution of both GP-zones and the β'-Mg_7Nd phases while coarse precipitates of β_1-Mg_3Nd phase formed [16].

It is worth noting that the β_e-$Mg_{41}Nd_5$ equilibrium phase was not observed during *in situ* ageing at 250 °C up to 5 h. Indeed, it was reported that the β_e-$Mg_{41}Nd_5$ phase could be observed only after annealing at higher temperatures (>500 °C) [23]. In fact, the temperature associated with the solubility limit for a nominal alloy concentration of 1.43% (wt.%) Nd is around 480 °C [24] and this suggests that the precipitation of β_e-$Mg_{41}Nd_5$ phase is possible below 500 °C. However, published XRD patterns of Mg-0.5Nd (at. %) (~2.35 wt.%) solution treated at 530 °C for 12 h fail to show any peak for the $Mg_{41}Nd_5$ phase [25] and some recent reports consider that $Mg_{12}Nd$ is effectively the ultimate phase, or equilibrium phase, in the precipitation sequence of the Mg–Nd alloy instead of the $Mg_{41}Nd_5$ phase [6, 20, 26].

The present results in Figs 2 and 3 show that during *in situ* ageing the β_1-Mg_3Nd is unstable while β-$Mg_{12}Nd$ is more stable in Mg-1.43Nd (wt.%) after HPT processing up to 10 turns. It may be possible that certain alloying elements and impurities such as oxygen could stabilize metastable phases or dislocations can nucleate a certain metastable phase despite the values of heat of formation. The present study seems to corroborate this statement owing to the high level of introduced dislocations HPT processing.

However, contradictory results were reported from theoretical predictions of phase stability [27] that revealed that β-$Mg_{12}Nd$ is the most unstable. The difficulty in the formation of intermetallic compounds may be directly represented by the formation heat where the

strongest negative value is indicative of an easier formation. Then the predicted binding energies of the intermetallic compounds reveal that β-$Mg_{12}Nd$ is the most unstable. These controversies between the current results and earlier proposals [27] may arise from the difficulty that all first principle calculations are necessarily undertaken at a temperature of absolute zero.

It is well established that the SPD processing of alloys after solution annealing leads to very rapid precipitation [28]. In fact, the application of SPD leads not only to substantial grain refinement but also to a high density of dislocations and vacancies that will enhance the atomic mobility and act as nucleation sites for precipitation. For example, it was observed that the presence of a high dislocation density significantly accelerates the precipitate formation kinetics [19]. Moreover, a reduction in the precipitation temperature after ECAP processing has been reported in the Cu-Cr-Zr system [29]. In this case, the precipitation of the Cu_3Zr phase was observed at 370 °C instead of 520 °C for the non-deformed sample [29]. However, in the present investigation using HPT processing up to 10 turns there was no evidence for such a drastic decrease in the β_e-$Mg_{41}Nd_5$ equilibrium phase precipitation temperature because the β_e-$Mg_{41}Nd_5$ equilibrium phase was not detected during *in situ* ageing at 250 °C up to 5 h. Furthermore, Kilbius et al [30] have shown that ageing of Mg-1.2Gd-2.7Nd-0.49Zr (wt.%) alloy at 250 °C for four hours caused formation of the equilibrium β_e-$Mg_{41}Nd_5$ phase. This alloy has a very similar decomposition sequence as the presently studied alloy but was aged after solution annealing and quenching and hence was expected to have moderate level of dislocations. This is not the case in the present study where the SPD processing is known to introduce considerable amount of defects ($> 10^{14}$ m^{-2}) [31]. It can be assumed hence, that the dislocations do not influence the kinetics of equilibrium phases such as β_e-$Mg_{41}Nd_5$ very effectively that it takes a very long time to transform mainly due to kinetic reasons.

The activation energies for the β'''phase, β_1-Mg_3Nd and β-$Mg_{12}Nd$ precipitate phases were found to be higher than that the lattice diffusion of Mg (135 kJ mol^{-1}) [32] except for the β'''phase after 10 HPT turns which gave a lower value of ~126 kJ mol^{-1}. Very scarce data about the activation energies associated with solid-state phase transformations in Mg-RE alloys exist in the literature. Only Nie et al. [2] and Riontino et al. [33] derived activation energy values for Mg-0.5Nd and WE54 alloys, respectively that were close to the present ones. Indeed, the values of the activation energies for different phase precipitation show an overall slight decrease of the activation energy with the amount of deformation introduced into the material by increasing the numbers of HPT turns. The β_1-Mg_3Nd and β-$Mg_{12}Nd$ phases showed the smallest and largest decreases, respectively. The activation energies for the analyzed phases indicate an almost diffusion-controlled process of precipitation that is influenced by the amount of defects introduced upon HPT processing. However, the activation energies summarized in Table 1 are comparable to those reported in an earlier investigation without SPD processing [6] which suggests that the use of SPD does not significantly affect the activation energy of the pre-precipitation process in the Mg-1.43Nd (wt.%) alloy. In this earlier work [6], the precipitate nature and crystallography were not fully established as well as the precipitation sequence and kinetics of an Mg-0.5Nd (at.%) alloy that was solution-annealed and aged at temperatures of 300–320 °C. It was suggested that the possible mechanism for the formation of different precipitation phases was the diffusion of solute atoms in the Mg matrix assisted by the abundant quench-in vacancies [6]. Similar result was also reported for the formation of the β_1 (183 kJ mol^{-1}) and β (177 kJ mol^{-1}) phases of the WE43 (Mg-4Y-3Nd, (wt.%)) alloy [33] and this may account for the slow kinetics of the phase transformations commonly accepted for Mg-RE alloys.

It seems also very probable that a nucleation-controlled mechanism could occur where the activation energy for nucleation decreases as dislocation sites are increased. This is very

probable since nucleation may occur both on dislocations and on precipitate/matrix misfit zones (formation of misfit defects at interphase boundaries). Furthermore, Choudhuri et al. [19] have studied the precipitate evolution within the a-Mg matrix of a HPDC Mg–Nd alloy during isothermal annealing at 177 °C by coupling detailed TEM studies with atom probe tomography. They evidenced that dislocations facilitated the formation of β'-Mg_7Nd and β_1-Mg_3Nd phases preferentially via heterogeneous nucleation coupled with accelerated diffusion of Nd along the dislocation lines (short-circuit paths). However, they did not reveal any precipitation of β-$Mg_{12}Nd$ phase. In the present study, it obviously seems that the β-$Mg_{12}Nd$ nucleation and growth are most sensitive to high density of dislocations.

4.2. Precipitation kinetics of β-$Mg_{12}Nd$ during aging

The isothermal kinetics of phase transformations in solid materials which proceed by nucleation and growth mechanisms can be described by the Johnson-Mehl-Avrami equation [34]:

$$X = 1 - \exp(-kt^n) \tag{2}$$

where t is the annealing time, k is a time constant and n is a coefficient that characterizes the transformation process. The fraction transformed, X, can be defined as:

$$X = \frac{I(t)}{I_f} \tag{3}$$

where $I(t)$ is the integrated intensity for a given reflection of the β-$Mg_{12}Nd$ phase (2θ = 15.32°) as a function of the annealing time and I_f is the intensity when the whole sample is transformed.

Figure 6 presents the evolution of $ln[ln((1-X)^{-1})]$ as function of $ln(t)$ for the β-$Mg_{12}Nd$ phase upon *in situ* aging at 250 °C of Mg-1.43Nd (wt.%) alloy after HPT processing to 1 and 10 turns. The values of the Avrami exponent, n, calculated from the slopes of the experimental data are equal to 0.95 and 1.10 for the Mg-1.43Nd (wt.%) alloy after HPT

processing to 1 turn and 10 turns, respectively. Thus, the values of the Avrami exponent are close to 1.

According to the theoretical values tabulated by Christian [35], these results indicate that the reaction of the precipitation corresponds to a process of grain boundary nucleation after site saturation and growth of the particles in 2 dimensions. Similar results for the Avrami exponent value (1.00 ± 0.04) were also reported for Mg-0.5Nd (at.%) aged at temperatures of 300–320 °C and this was explained by growth of particles in two dimensions [6]. The results do not fit a dislocation-based nucleation which Avrami exponent stated a value equal to 2/3 [35]. However, it is to be noted that many studies evidenced progressive transformation of cell boundaries (formed of tangled dislocations) or sub-grain boundaries (formed of well-ordered dislocations) into high angle grain boundaries during severe plastic deformation (SPD) and subsequent ageing [11–13, 36]. Ultra-fine grained materials obtained by SPD processing have a main feature that is the existence of a significant volume fraction of grain boundaries. It results in a number of unusual physical properties and high abnormal diffusion activity [37]. It is reasonable to conclude, therefore, that HPT processing does not significantly alter the nucleation mechanisms as well as the kinetics of the β-$Mg_{12}Nd$ phase during *in situ* aging at 250 °C.

5. Summary and conclusions

1. After *in situ* aging of an Mg-1.43Nd (wt.%) alloy at 250°C for up to 5 hours after processing by HPT, it is shown that there is no evidence for the metastable β’’’phase and β$'$-Mg_7Nd phase or for the equilibrium β_e-$Mg_{41}Nd_5$ phase. The β_1-Mg_3Nd and β-$Mg_{12}Nd$ phases appeared more rapidly after HPT processing compared to the non-deformed state.

2. The amount of β_1-Mg_3Nd and β-$Mg_{12}Nd$ phases was larger after HPT processing compared to the non-deformed sample and increased with increasing strain. The Avrami time

exponent of the β-$Mg_{12}Nd$ precipitation was close to unity and suggested a mechanism of nucleation after site saturation and growth of the particles in 2 dimensions. Processing by HPT did not alter the nucleation mechanisms as well as the kinetics of the β-$Mg_{12}Nd$ phase during aging at 250 °C.

3. A DSC analysis of the Mg-1.43Nd (wt.%) alloy after SPD by HPT revealed the sequence of pre-precipitation of metastable phases as well as the equilibrium phase using a heating rate of 30°C/min. The activation energy associated with the pre-precipitation of β”’ (undifferentiated β”-Mg_3Nd and β’-Mg_7Nd), β_1-Mg_3Nd and β-$Mg_{12}Nd$ phases ranged from ~126 to ~235 kJ mol^{-1}. The energy decreased with the amount of deformation introduced into the material with increasing HPT turns. The results reveal an almost diffusion-controlled process of precipitation that is influenced by the density of defects introduced during HPT processing.

Acknowledgements

D.B. gratefully acknowledges the support of the SOLEIL synchrotron facility while performing the experiments through the 20150973 proposal. Y.I.B wishes to heartily thank Pr. Jose Maria CABRERA from Polytecnia ETSEIB, Universidad Politécnica de Cataluña (UPC), for inviting and helping him during his scientific stay and Mr. Jairo Alberto Muñoz and the Biomaterials research group of UPC for their support in the DSC analysis. YH and TGL were supported by the European Research Council under ERC Grant Agreement No. 267464-SPDMETALS.

References

[1] B.L. Mordike. Creep-resistant magnesium alloys. Mater. Sci. Eng. A 324 (2002) 103–112.

[2] J.F. Nie, Precipitation and hardening in magnesium alloys, Metall. Mater. Trans. A 43 (2012) 3891–3939.

[3] I. Basu, T. Al-Samman, Deformation, Recrystallization and Grain Growth Behavior of Large-Strain Hot Rolled Binary Mg-1Dy Alloy, in Magnesium Technology 2014 (eds M. Alderman, M. V. Manuel, N. Hort and N. R. Neelameggham), John Wiley & Sons, Inc., Hoboken, NJ, USA.

[4] S.M. Zhu, M.A. Gibson, M.A. Easton, J.F. Nie. The relationship between microstructure and creep resistance in die-cast magnesium–rare earth alloys. Scripta Mater. 63 (2010) 698–703.

[5] M.O. Pekguleryuz, A. Kaya. Creep Resistant Magnesium Alloys for Powertrain Applications. Adv. Eng. Mater. 5 (2003) 866–878.

[4] Y.Z. Ji, A. Issa, T.W. Heo, J.E. Saal, C. Wolverton, L.Q. Chen. Predicting β’ precipitate morphology and evolution in Mg–RE alloys using a combination of first-principles calculations and phase-field modeling, Acta Mater. 76 (2014) 259–271.

[6] T.J. Pike, B. Noble. The formation and structure of precipitates in a dilute magnesium-neodymium alloy. J. Less-Common Met. 30 (1973) 63–73.

[7] R.Z. Valiev, T.G. Langdon, Principles of equal-channel angular pressing as a processing tool for grain refinement. Prog. Mater. Sci. 51 (2006) 881-981.

[8] Y. Saito, N. Tsuji, H. Utsunomiya, T. Sakai, R.G. Hong. Ultra-fine grained bulk aluminum produced by accumulative roll-bonding (ARB) process. Scripta Mater. 39, (1998) 1221–1227.

[9] A.P. Zhilyaev, T.G. Langdon, Using high-pressure torsion for metal processing: Fundamentals and applications. Prog. Mater. Sci. 53 (2008) 893-979.

[10] T.G. Langdon, Twenty-five years of ultrafine-grained materials: Achieving exceptional properties through grain refinement. Acta Mater. 61 (2013) 7035–7059.

[11] A. Y. Khereddine, F. Hadj Larbi, H. Azzeddine, T. Baudin, F. Brisset, A.L. Helbert, M.H. Mathon, M. Kawasaki, D. Bradai, T. G. Langdon. Microstructures and Textures of a Cu-Ni-Si Alloy Processed by High-Pressure Torsion. J. Alloys Compds 574 (2013) 361–367.

[12] K. Tirsatine, H. Azzeddine, T. Baudin, A-L Helbert, F. Brisset, B. Alili, D. Bradai. Texture and microstructure evolution of Fe-Ni alloy after Accumulative Roll Bonding. J. Alloys Compds 610 (2014) 352–360.

[13] F. Hadj Larbi, H. Azzeddine, T. Baudin, M-H. Mathon, F. Brisset, A-L. Helbert, M. Kawasaki, D. Bradai, T.G. Langdon. Microstructure and texture evolution in a Cu-Ni-Si alloy processed by equal-channel angular pressing. J. Alloys Compd. 638 (2015) 88–94.

[14] J. Gubicza, I. Schiller, N.Q. Chinh, J. Illy, Z. Horita, T.G. Langdon. The effect of severe plastic deformation on precipitation in supersaturated Al–Zn–Mg alloys. Mater. Sci. Eng. A 460–461 (2007) 77–85.

[15] H. Azzeddine, B. Mehdi, T. Baudin, A-L. Helbert, F. Brisset, D. Bradai**.** An in situ synchrotron X-ray diffraction study of precipitation kinetics in a severely deformed Cu-Ni-Si alloy. Mater. Sci. Eng. A597 (2014) 288–294.

[16] K. Saito, K. Hiraga. The structures of precipitates in an Mg-0.5 at%Nd age-hardened alloy studied by HAADF-STEM Technique. Mater. Trans. 52 (2011) 1860–1867.

[17] A. R. Natarajan, E. L.S. Solomon, B. Puchala, E. A. Marquis, A. Van der Ven. On the early stages of precipitation in dilute Mg–Nd alloys. Acta Mater. 108 (2016) 367–379.

[18] L.Y. Wei, G.L. Dunlop, H. Westengen. Age hardening and precipitation in a cast magnesium-rare-earth alloy. J. Mater. Sci., 31 (1996) 387–97.

[19] D. Choudhuri, N. Dendge, S. Nag, S. Meher, T. Alam, M. A. Gibson, R. Banerjee. Homogeneous and heterogeneous precipitation mechanisms in a binary Mg–Nd alloy. J. Mater. Sci. 49 (2014) 6986–7003.

[20] A. Sanaty-Zadeh, A. A. Luob, D. S. Stone. Comprehensive study of phase transformation in age-hardening of Mg–3Nd–0.2Zn by means of scanning transmission electron microscopy. Acta Mater. 94 (2015) 294–306.

[21] R.B. Figueiredo, P.H.R. Pereira, M.T.P. Aguilar, P.R. Cetlin, T.G. Langdon, Using finite element modeling to examine the temperature distribution in quasi-constrained high-pressure torsion, Acta Mater. 60 (2012) 3190–3198.

[22] P.G. Boswell. On the calculation of activation-energies using a modified Kissinger method. J. Therm. Anal. 18 (1980) 353–358.

[23] M.A. Easton, M.A. Gibson, D. Qiu, S.M. Zhu, J. Grobner, R. Schmid-Fetzer, J.F. Nie, M.X. Zhang. The role of crystallography and thermodynamics on phase selection in binary magnesium–rare earth (Ce or Nd) alloys. Acta Mater. 60 (2012) 4420–4430.

[24] L. L. Rokhlin. Magnesium alloys containing rare earth metals: structure and properties. Advances in Metallic Alloys, vol. 3, Taylor & Francis, London, 2003.

[25] C. Su, D. Li, T. Ying, L. Zhou, L. Li, X. Zeng. Effect of Nd content and heat treatment on the thermal conductivity of Mg–Nd alloys. J. Alloys Compds 685 (2016) 114–121.

[26] L.Y. Wei. Age hardening and precipitation in a cast magnesium-rare-earth alloy. J. Mater. Sci. 31 (1996) 387–397.

[27] W. Can, H. Peide, Z. Lu, Z. Caili, X. Bingshe. First-principles study on the stabilities of the intermetallic compounds in Mg-Nd alloys. Rare Metal Mater. Eng. 40 (2011) 590–594.

[28] G. Sha, Y.B. Wang, X.Z. Liao, Z.C. Duan, S.P. Ringer, T.G. Langdon. Influence of equal-channel angular pressing on precipitation in an Al–Zn–Mg–Cu alloy. Acta Mater. 57 (2009) 3123–3132.

[29] A. Vinogradov, Y. Suzuki, T. Ishida, K. Kitawaga, V. I. Kopylov. Effect of chemical composition on structure and properties of ultrafine grained Cu-Cr-Zr alloys produced by equal-channel angular pressing. Mater. Trans. 45 (2004) 2187–2191.

[30] A. Kielbus, T. Rzychon, L. Litynska-Dobrzynska, G. Dercz. Characterization of β and $Mg_{41}Nd5$ equilibrium phases in Elektron 21 magnesium alloy after long-term annealing. Solid State Phenomena 163 (2010) 106–109.

[31] M. Janecek, J. Cizek, J. Gubicza, J. Vratna. Microstructure and dislocation density evolutions in MgAlZn alloy processed by severe plastic deformation. J Mater Sci 47 (2012 7860–7869.

[32] H.J. Frost, M.F. Ashby, Deformation Mechanism Maps, Pergamon Press, Oxford, 1982.

[33] G. Riontino, D. Lussana and M. Massazza. A calorimetric study of phase evolution in a WE43 Mg alloy. J. Thermal Anal. Calorim. 83 (2006) 643–647.

[34] M. Avrami. Granulation, phase change and microstructure: Kinetics of phase change III. J. Chem. Phys. 7 (1941) 184–177.

[35] J.W. Christian. The Theory of Transformations in Metals and Alloys. Pergamon Press, London; 1965.

[36] F.J. Humphreys, M. Hatherly. Recrystallisation and related Annealing Phenomena, Pergamon, Oxford, UK (1995).

[37] J. Čížek, I. Procházka, G. Brauer, W. Anwand, R. Kužel, M. Cieslar, and R. K. Islamgaliev. Spatial distribution of defects in ultra-fine grained copper prepared by high-pressure torsion. Physica Status Solidi A-Applied Research, 195 (2003) 335–349.

Figure captions

Figure 1: X-ray diffraction patterns of the non-deformed Mg-1.43Nd (wt.%) alloy after solution annealing at 535 °C for 6 h and *in situ* ageing at 250 °C to 5 h.

Figure 2: X-ray diffraction patterns of the Mg-1.43Nd (wt.%) after HPT processing to 1 turn, obtained during *in situ* ageing at 250 °C to 5 h: a) 2D and b) the integrated pattern.

Figure 3: X-ray diffraction patterns of the Mg-1.43Nd (wt.%) after HPT processing to 10 turns, obtained during *in situ* ageing at 250 °C to 5 h: a) 2D and b) the integrated pattern.

Figure 4: DSC curves of Mg-1.43Nd (% wt.) after annealing at 523 °C for 6 h and processing by HPT after 1 and 10 turns, scanned at a heating rate of 30 °C/min.

Figure 5: Boswell plots for Mg-1.43Nd (% wt.) deformed by HPT up to 1 and 10 turns for: (a) β''' phase, (b) β_1-Mg_3Nd and (c) β-$Mg_{12}Nd$.

Figure 6: Evolution of $ln[ln((1-X)^{-1})]$ as function of $ln(t)$ for the β-$Mg_{12}Nd$ phase observed at *in situ* aged at 250 °C on the Mg-1.43Nd (wt.%) alloy after HPT processing to (a) 1 turn and (b) 10 turns.

Table 1: Activation energies (kJ mol^{-1}) for different precipitate phases: data from [5] shown for comparison.

Sample	β‴ phase	β_1-Mg_3Nd	β-$Mg_{12}Nd$
Mg-1.43Nd (wt.%) 1 turn	140	148	235
Mg-1.43Nd (wt.%) 10 turns	126	147	166
Mg-0.5Nd (at.%)	153	146	145 [5]

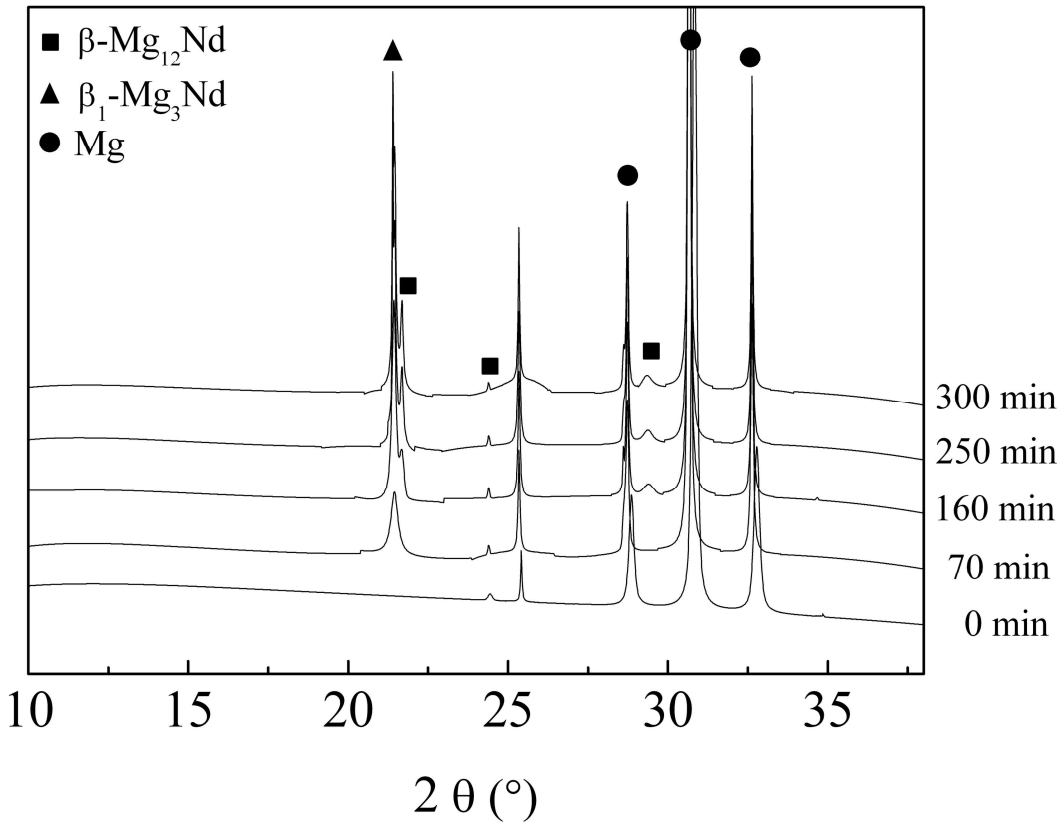

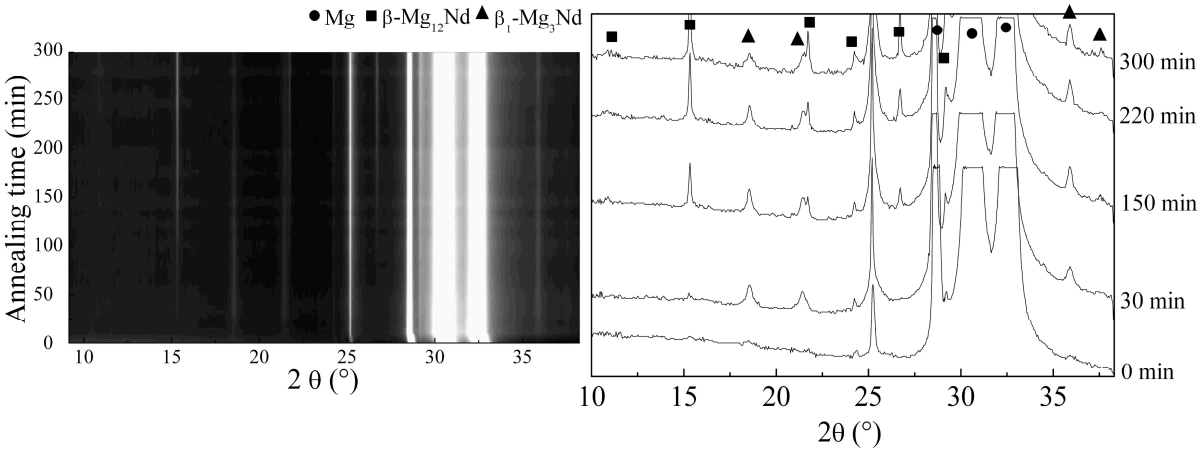

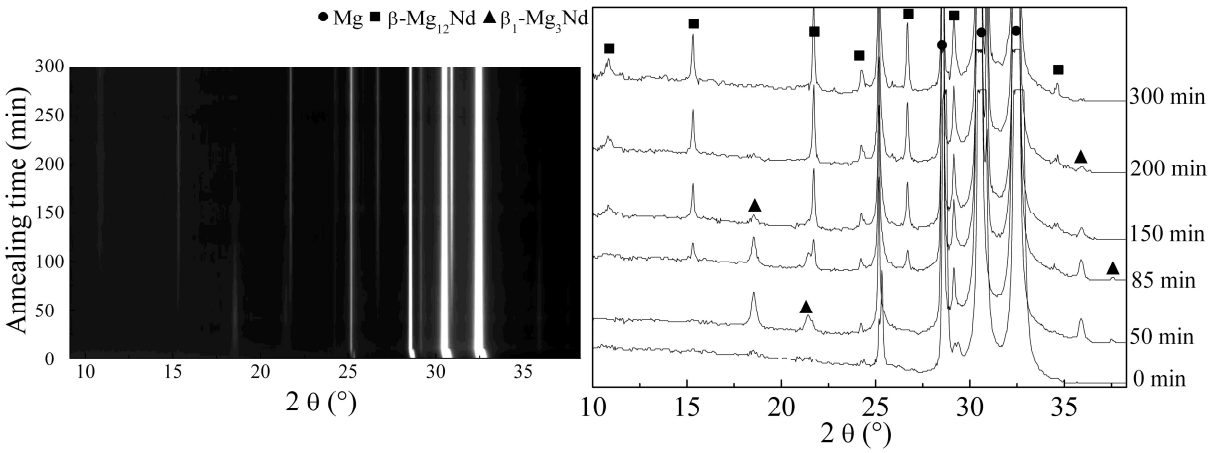

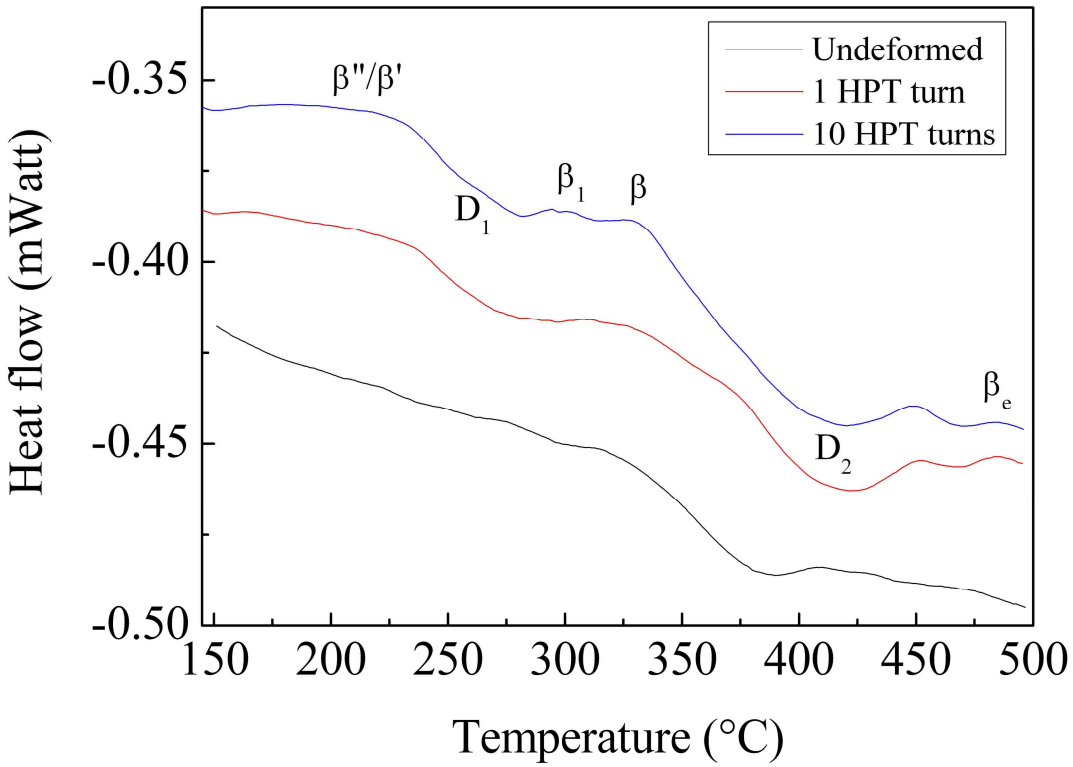

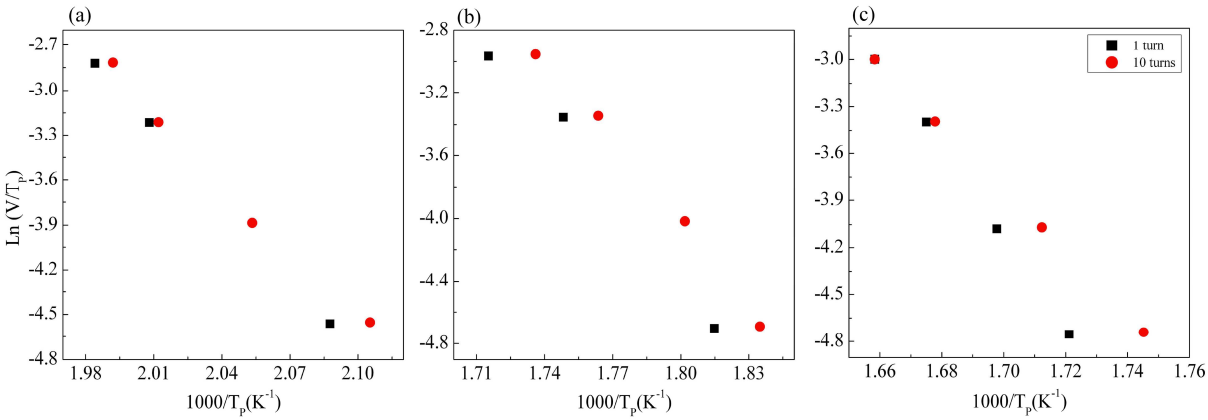

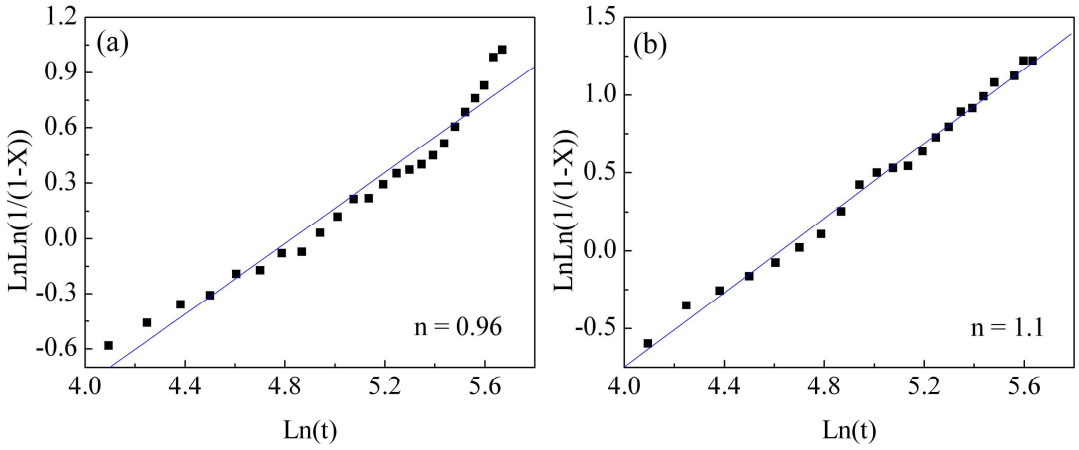

Highlight

No evidence for the β’’’phase and Mg_7Nd phase or for the equilibrium $Mg_{41}Nd_5$ phase.

The β_1-Mg_3Nd and β-$Mg_{12}Nd$ phases appeared more rapidly after HPT processing.

The Avrami time exponent of the β-$Mg_{12}Nd$ precipitation was close to unity.

The activation energy of the pre-precipitation phases ranged from 126–235 kJ mol^{-1}.

The results reveal an almost diffusion-controlled process of precipitation.